PROCEEDINGS OF SCIENCE

Study of the decay $B_d^0 \to K^{*0}\mu^+\mu^-$ in ATLAS

Semen Turchikhin*, on behalf of the ATLAS collaboration
Skobeltsyn Institute of Nuclear Physics, Lomonosov Moscow State University;
also at Lomonosov Moscow State University, Faculty of Physics
E-mail: Semen.Turchikhin@cern.ch

A measurement of the muon forward-backward asymmetry A_{FB} and the longitudinal polarization fraction F_L of K^{*0} in the decay $B_d^0 \to K^{*0}\mu^+\mu^-$ as functions of the di-muon invariant mass squared is presented. A data sample of 4.9 fb^{-1} integrated luminosity collected with the ATLAS detector at the Large Hadron Collider in pp collisions at a centre of mass energy $\sqrt{s} = 7$ TeV is used. The measurement is compared to the Standard Model predictions and the results of other experiments.

XXI International Workshop on Deep-Inelastic Scattering and Related Subjects
22-26 April, 2013
Marseilles, France

*Speaker.

© Copyright owned by the author(s) under the terms of the Creative Commons Attribution-NonCommercial-ShareAlike Licence. http://pos.sissa.it/

PoS(DIS 2013)188

1. Introduction

The $B_d^0 \to K^{*0}\mu^+\mu^-$ decay provides an exclusive final state for the $b \to s\ell^+\ell^-$ transition that occurs only via loop diagrams within the Standard Model (SM) and therefore has a small branching fraction of $(1.06 \pm 0.10) \cdot 10^{-6}$ [1]. The decay amplitudes and the final state particles angular distributions are shown to be sensitive to physics beyond the SM [2].

The kinematics of the $B_d^0 \to K^{*0}\mu^+\mu^-$ decay with $K^{*0} \to K^+\pi^-$ (charge conjugate modes are implied unless otherwise stated) is described in terms of four variables, one is the di-muon invariant mass squared q^2, the other three are the angles describing the final state geometrical configuration as shown in Fig. 1: θ_L is the angle between the μ^+ (μ^-) momentum and the direction opposite to the B_d^0 ($\bar{B}_d^0$) in the di-muon rest frame, θ_K is the angle between the K^+ (K^-) momentum and the direction opposite to the B_d^0 ($\bar{B}_d^0$) in the K^{*0} ($\bar{K}^{*0}$) rest frame, and ϕ is the angle between the two planes defined by the muon pair and by the $K^+\pi^-$ ($K^-\pi^+$) system in the B_d^0 ($\bar{B}_d^0$) rest frame.

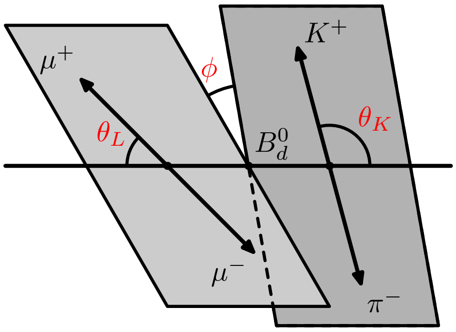

Figure 1: Illustration of the kinematic angles definition.

When the experimental statistics is insufficient to study the 4-differential decay rate, two of the three angles can be integrated out resulting in the 2-dimensional distributions $\mathrm{d}^2\Gamma/\mathrm{d}q^2\mathrm{d}\cos\theta_L$ and $\mathrm{d}^2\Gamma/\mathrm{d}q^2\mathrm{d}\cos\theta_K$. The forward-backward asymmetry of the muons A_{FB} and the fraction of K^{*0} longitudinal polarization can be extracted from the fit to 1-dimensional angular distributions while the q^2 dependence is accounted for by performing a fit separately in several ranges of q^2.

This measurement was previously performed by BaBar [3, 4], Belle [5], CDF [6] and LHCb [7]. In this work the measurement of A_{FB} and F_L as functions of q^2 in the ATLAS experiment at the LHC is presented [8].

2. Event selection

The data sample corresponding to 4.9 fb^{-1} integrated luminosity of pp collisions at $\sqrt{s} =$ 7 TeV collected by the ATLAS detector in 2011 is used in this analysis. The detailed description of the experimental facility can be found elsewhere [9]. Several triggers based on either single muon or di-muon signatures have been used for online event selection.

The Monte Carlo (MC) event samples used in the analysis have been generated with PYTHIA 6 and include the signal decay channel $B_d^0 \to K^{*0}\mu^+\mu^-$, the resonant background decay channel $B_d^0 \to K^{*0}J/\psi$, the Drell-Yan process and the processes $b\bar{b} \to \mu^+\mu^-X$ and $c\bar{c} \to \mu^+\mu^-X$ contributing to the continuum background.

PoS(DIS 2013)188

A first set of cuts has been applied to the data in order to perform the initial skim of the sample and ensure good measurement quality. All four tracks forming the signal decay candidate are required to have pseudorapidity $|\eta| < 2.5$, the transverse momentum p_T of muon tracks to be above 3.5 GeV, and p_T of hadron tracks above 0.5 GeV. The muon track pair must be successfully fitted to a common vertex satisfying $\chi^2/\text{n.d.f.} < 10$. The mass of the K^{*0} candidate formed of two tracks must be between 846 MeV and 946 MeV (as pions and kaons are not distinguished, both mass hypotheses are tested). To avoid background from events with a muon pair originating from J/ψ or $\psi(2S)$ decay, the di-muons in mass regions $\pm 3\sigma$ around the charmonia PDG masses are excluded, where σ is mass resolution varying throughout the detector volume.

Further selection criteria are optimized by maximizing the estimator $\mathscr{P} = N_{\text{sig}}/\sqrt{N_{\text{sig}} + N_{\text{bkg}}}$, where N_{sig} and N_{bkg} are the numbers of signal and background events surviving the selection, respectively. The optimisation is performed using MC events only, where the MC samples are reweighted according to their cross-sections.

A cut on the B_d^0 candidate lifetime significance $\tau/\sigma_\tau > 12.75$ is applied to remove most of $b\bar{b} \to \mu^+\mu^- X$, $c\bar{c} \to \mu^+\mu^- X$ and Drell-Yan events. To further suppress the combinatorial background the quality of the fitted vertex of the B_d^0 candidate is required to satisfy $\chi^2/\text{n.d.f.} < 2$ and a cut on the pointing angle $\cos\theta > 0.999$ is imposed, where the pointing angle θ is defined as the angle between the B_d^0 candidate momentum vector and the vector between the primary vertex and secondary B_d^0 vertex. To remove the background events with K^{*0} candidates not originating from a B decay, a cut on its transverse momentum $p_T(K^{*0}) > 3.0$ GeV is applied. Finally, to suppress the decays $B_d^0 \to K^{*0} J/\psi$ and $B_d^0 \to K^{*0}\psi(2S)$ with subsequent radiative decays of charmonia (e. g. $J/\psi \to \mu^+\mu^-\gamma$ or $\psi(2S) \to \mu^+\mu^-\gamma$) as well as remaining J/ψ and $\psi(2S)$ in the tails of their peaks, a cut $\Delta M < 130$ MeV is introduced, where $DeltaM = \left|\left(m(B_d^0)_{rec} - m(B_d^0)_{PDG}\right) - \left(m(\mu^+\mu^-)_{rec} - m(c\bar{c})_{PDG}\right)\right|$ with $c\bar{c}$ denoting either J/ψ or $\psi(2S)$. The mass distribution of the B_d^0 candidates passing the selection cuts is shown in Fig. 2.

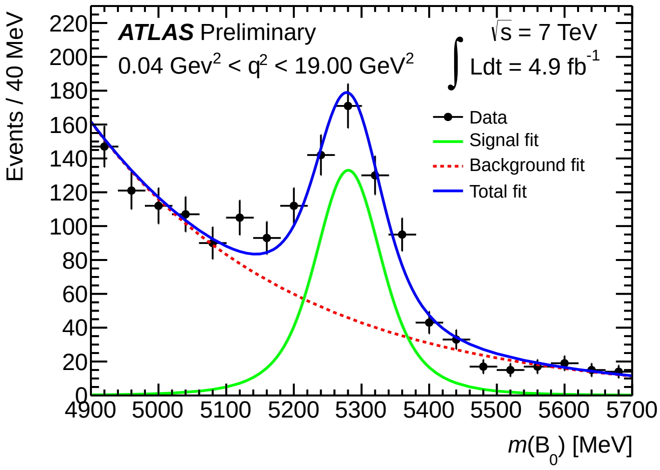

Figure 2: Invariant mass distribution of $B_d^0 \to K^{*0}\mu^+\mu^-$ candidates as data points after the full signal selection. The solid blue (dark) line denotes the mass likelihood fit, the dotted red line is its background component and the solid green (light) line is the signal component. Figure taken from [8].

PoS(DIS 2013)188

3. Measurement of A_{FB} and F_L

To measure the lepton forward-backward asymmetry A_{FB} and the longitudinal polarization fraction F_L as functions of di-muon invariant mass q^2 the data sample is divided into several regions of q^2. The values of A_{FB} and F_L are extracted by performing a sequential unbinned maximum likelihood fit, where in a first step the B_d^0 candidate mass distribution is fitted, and in a second step the angular distributions are fitted while the signal and background yields are fixed by the previous mass fit. For the invariant mass fit the following likelihood function is used

$$\mathscr{L} = \prod_{i=1}^{N} \left[N_{\text{sig}} \cdot \mathscr{M}_{\text{sig}}(m_i, \delta_{m_i}) + N_{\text{bckg}} \cdot \mathscr{M}_{\text{bckg}}(m_i) \right], \tag{3.1}$$

where N_{sig} (N_{bckg}) is the number of signal (background) events and $\mathscr{M}_{\text{sig}}$ ($\mathscr{M}_{\text{bckg}}$) is the probability density function for signal (background). For the signal a Gaussian function with mass m_i and per-candidate mass error δm_i is used, while the background is modelled with an exponential.

The differential decay rate is parametrized by the di-muon invariant mass squared q^2 and the three helicity angles θ_L, θ_K and ϕ defined above. Its integration over θ_K and ϕ at a given q^2 gives [10, 11]

$$\frac{1}{\Gamma}\frac{\mathrm{d}^2\Gamma}{\mathrm{d}q^2\mathrm{d}\cos\theta_L} = \frac{3}{4}F_L(q^2)(1-\cos^2\theta_L) + \frac{3}{8}(1-F_L(q^2))(1+\cos^2\theta_L) + A_{FB}(q^2)\cos\theta_L \tag{3.2}$$

and the integration over θ_L and ϕ gives

$$\frac{1}{\Gamma}\frac{\mathrm{d}^2\Gamma}{\mathrm{d}q^2\mathrm{d}\cos\theta_K} = \frac{3}{2}F_L(q^2)\cos^2\theta_K + \frac{3}{4}(1-F_L(q^2))(1-\cos^2\theta_K). \tag{3.3}$$

The likelihood function for the angular distribution after fixing the parameters obtained from the mass fit can be written as

$$\begin{aligned}\mathscr{L} = \prod_{i=1}^{N} [N_{\text{sig}}^{fix} \cdot \mathscr{M}_{\text{sig}}(m_i, \delta_{m_i}|\text{fixed}) \cdot \mathscr{A}_{L,\text{sig}}(\cos\theta_{L,i}) \cdot \alpha_L(\cos\theta_{L,i}) \cdot \mathscr{A}_{K,\text{sig}}(\cos\theta_{K,i}) \cdot \alpha_K(\cos\theta_{K,i}) + \\ N_{\text{bckg}}^{fix} \cdot \mathscr{M}_{\text{bckg}}(m_i|\text{fixed}) \cdot \mathscr{A}_{L,\text{bckg}}(\cos\theta_{L,i}) \cdot \mathscr{A}_{K,\text{bckg}}(\cos\theta_{K,i})],\end{aligned} \tag{3.4}$$

where $\mathscr{A}$'s denote the probability density functions of $\cos\theta_K$ and $\cos\theta_L$ distributions for the signal and the background. The angular distributions of the signal are given by Eq. 3.2 and 3.3, while those for the background are modelled with the linear combinations of Chebyshev polynomials up to second order. The α_L and α_K are the angular acceptance functions introduced to take into account the effect of the detector, trigger, event reconstruction and selection efficiencies on the signal angular shapes. To determine these functions a signal MC sample with full detector simulation and uniform distribution of the helicity angles has been used. Uncertainties in these acceptance functions are included in systematic errors.

4. Systematics

Various sources of systematic uncertainties have been studied, evaluated separately for each q^2 region.

PoS(DIS 2013)188

The uncertainty due to sequential fitting procedure has been estimated by comparing the fit result with that of the simultaneous mass-angular fit. The deviations in the B_d^0 mass fit due to the $\Delta M > 130$ MeV cut are accounted for by varying the ranges of the fit region. A small systematic uncertainty has been assigned due to the variation of the background angular shape description. Several possible effects related to the angular acceptance functions have been studied, including variations due to limited statistics of the MC sample used, effect of correlations among the full three angles, and the effect of acceptance and resolution in the di-muon mass.

The contamination of the signal by $B^\pm \to K^\pm\mu^+\mu^-$ decays has been conservatively estimated by removing all potential $B^\pm$ candidates which could be formed from the di-muon and either charged hadron. The contaminations by the $B_s^0 \to \phi\mu^+\mu^-$ decay as well as the S-wave $B_d^0 \to K^+\pi^-\mu^+\mu^-$ decay are found to be negligible.

No common dominating source of systematic uncertainty for all of the q^2 regions has been found. The full uncertainties of A_{FB} and F_L are dominated with the statistical ones.

5. Results

The parameters A_{FB} and F_L are extracted in six ranges of q^2, which had been first introduced by Belle [5] and used in all later measurements. The final results including statistical and systematic uncertainties are shown in Table 1. No result is present in 0.04 GeV^2 to 2.00 GeV^2 because of the low statistics in that region. In Fig. 3 the ATLAS measurements are compared to the measurements of other experiments and the SM predictions.

Table 1: Summary of the fit results for different q^2 regions [8]. The number of signal events $N_{\rm sig}$ is shown with statistical uncertainty only. For the A_{FB} and F_L values the first uncertainty is statistical and the second is systematic.

q^2 range (GeV^2)	$N_{\rm sig}$	A_{FB}	F_L
$2.00 < q^2 < 4.30$	19 ± 8	$0.22 \pm 0.28 \pm 0.14$	$0.26 \pm 0.18 \pm 0.06$
$4.30 < q^2 < 8.68$	88 ± 17	$0.24 \pm 0.13 \pm 0.01$	$0.37 \pm 0.11 \pm 0.02$
$10.09 < q^2 < 12.86$	138 ± 31	$0.09 \pm 0.09 \pm 0.03$	$0.50 \pm 0.09 \pm 0.04$
$14.18 < q^2 < 16.00$	32 ± 14	$0.48 \pm 0.19 \pm 0.05$	$0.28 \pm 0.16 \pm 0.03$
$16.00 < q^2 < 19.00$	149 ± 24	$0.16 \pm 0.10 \pm 0.03$	$0.35 \pm 0.08 \pm 0.02$
$1.00 < q^2 < 6.00$	42 ± 11	$0.07 \pm 0.20 \pm 0.07$	$0.18 \pm 0.15 \pm 0.03$

The results of ATLAS are in general agreement with those of other experiments and no significant deviations from the theoretical expectations have been found.

References

[1] Particle Data Group, J. Beringer et al., Phys. Rev. D **86** (2012) 010001, `http://pdg.lbl.gov`

[2] T. Feldman and J. Matias, JHEP **0301** (2003) 074, `arXiv:hep-ph/0212158`

[3] BaBar Collaboration, Phys. Rev D **79** (2009) 031102, `arXiv:0804.4412`

[4] J. Ritchie, for the BaBar Collaboration, `arXiv:1301.1700`

PoS(DIS 2013)188

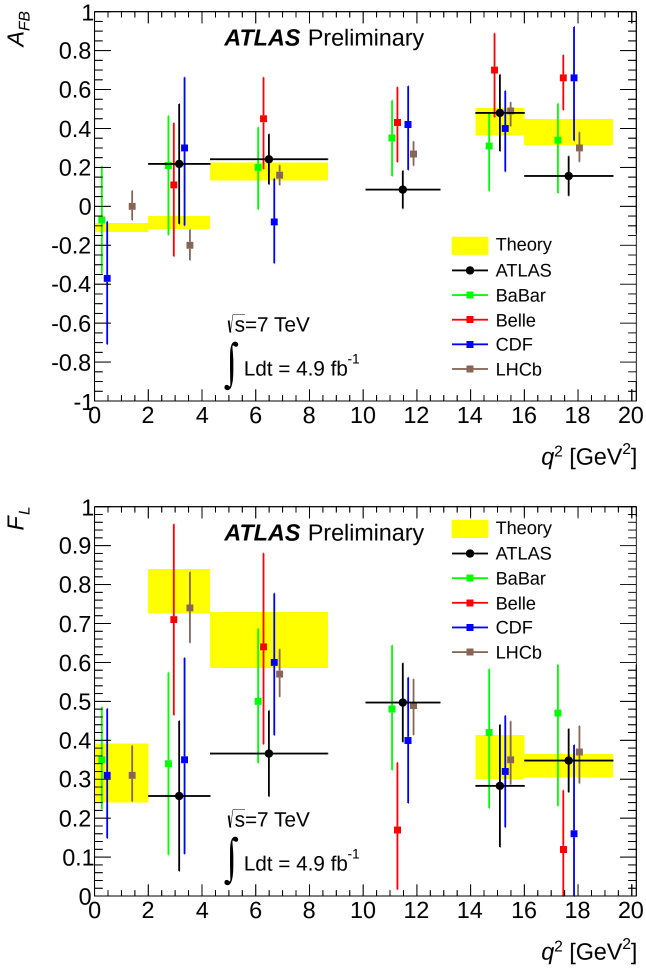

Figure 3: Muon forward-backward asymmetry A_{FB} (top) and the longitudinal polarization fraction F_L (bottom) including statistical and systematic uncertainties, compared to the theoretical predictions [12] and the results of BaBar [4], Belle [5], CDF [6] and LHCb [7]. Figure taken from [8].

[5] Belle Collaboration, Phys. Rev. Lett. **103** (2009) 171801, arXiv:0904.0770

[6] CDF Collaboration, Phys. Rev. Lett. **108** (2012) 081807, arXiv:1108.0695

[7] LHCb Collaboration, LHCb-CONF-2012-008, https://cds.cern.ch/record/1427691

[8] ATLAS Collaboration, ATLAS-CONF-2013-038, http://cds.cern.ch/record/1537961

[9] ATLAS Collaboration, JINST **3** (2008) S08003

[10] C. Bobeth, G. Hiller, D. van Dyk, Phys. Rev. D **87** (2012) 034016, arXiv:1212.2321

[11] F. Kruger, J. Matias, Phys. Rev. D **71** (2005) 094009, arXiv:hep-ph/0502060v2

[12] C. Bobeth, G. Hiller, D. van Dyk, DO-TH 11/02 (2011), arXiv:1105:2659v1

PoS(DIS 2013)188